



Possible jet contribution to the γ -ray luminosity in NGC 1068

Downloaded from: <https://research.chalmers.se>, 2024-08-26 13:16 UTC

Citation for the original published paper (version of record):

Salvatore, S., Eichmann, B., Rodrigues, X. et al (2024). Possible jet contribution to the γ -ray luminosity in NGC 1068. *Astronomy and Astrophysics*, 687.

<http://dx.doi.org/10.1051/0004-6361/202348447>

N.B. When citing this work, cite the original published paper.

Possible jet contribution to the γ -ray luminosity in NGC 1068

S. Salvatore^{1,2}, B. Eichmann^{1,2} , X. Rodrigues^{2,3,4} , R.-J. Dettmar^{2,4} , and J. Becker Tjus^{1,2,5} 

¹ Ruhr-Universität Bochum, Fakultät für Physik und Astronomie, Theoretische Physik IV, 44780 Bochum, Germany
e-mail: silvia.salvatore@rub.de

² Ruhr Astroparticle and Plasma Physics Center (RAPP Center), 44780 Bochum, Germany

³ European Southern Observatory, Karl-Schwarzschild-Straße 2, 85748 Garching bei München, Germany

⁴ Ruhr-Universität Bochum, Fakultät für Physik und Astronomie, Astronomisches Institut (AIRUB), 44780 Bochum, Germany

⁵ Department of Space Earth and Environment, Chalmers University of Technology, 412 96 Gothenburg, Sweden

Received 31 October 2023 / Accepted 10 April 2024

ABSTRACT

NGC 1068 is a nearby, widely studied Seyfert II galaxy presenting radio, infrared, X-ray, and γ -ray emission, along with strong evidence for high-energy neutrino emission. Recently, the evidence for neutrino emission was explained in a multimessenger model, whereby the neutrinos originate from the corona of the active galactic nucleus. In this environment, γ -rays are strongly absorbed, so that an additional contribution is necessary, for instance, from the circumnuclear starburst ring. In this work, we discuss whether the radio jet can be an alternative source of the γ -rays between about 0.1 and 100 GeV, as observed by *Fermi*-LAT. In particular, we include both leptonic and hadronic processes, namely, accounting for inverse Compton emission and signatures from pp as well as $p\gamma$ interactions. In order to constrain our calculations, we used VLBA and ALMA observations of the radio knot structures, which are spatially resolved at different distances from the supermassive black hole. Our results show that the best leptonic scenario for the prediction of the *Fermi*-LAT data is provided by the radio knot closest to the central engine. For that to be the case, a magnetic field strength of ~ 1 mG is needed as well as a strong spectral softening of the relativistic electron distribution at (1–10) GeV. However, we show that neither such a weak magnetic field strength, nor such a strong softening is expected for that knot. A possible explanation for the ~ 10 GeV γ -rays could potentially be provided by hadronic pion production in case of a gas density $\gtrsim 10^4$ cm⁻³. Nonetheless, this process is not found to contribute significantly to the low-energy end of the *Fermi*-LAT range. We conclude that the emission sites in the jet are not sufficient to explain the γ -rays across the whole *Fermi*-LAT energy band.

Key words. galaxies: Seyfert – gamma rays: general – X-rays: galaxies

1. Introduction

The nearby starburst-Seyfert II galaxy NGC 1068, located at a distance of $D_L = 10.1 \pm 1.8$ Mpc (Tully et al. 2009), is not only one of the first and brightest galaxies of its kind studied by Seyfert (1943) – but it is also one of the first sources to show strong evidence for neutrino emission, as observed by the IceCube experiment (Abbasi et al. 2022). NGC 1068 shows also clear non-thermal emission in the γ -ray band up to some tens of GeV (Ackermann et al. 2012). The observation of a neutrino flux that is much higher than the gamma-ray flux resulted in the expectation that neutrinos must be produced in a γ -ray absorbed environment (Inoue et al. 2020, 2022; Murase et al. 2020; Kheirandish et al. 2021; Eichmann et al. 2022). Since the AGN corona is optically thick to γ -rays, it seems to be the most likely origin of the TeV neutrinos. The origin of the GeV γ -rays is less clear, since it may be located in different regions. Eichmann et al. (2022) explore the possibility that γ -rays with energies higher than a few hundreds of MeV are produced by hadronic pion production in the starburst ring located ~ 1.3 pc from the BH. Another scenario, presented by Inoue et al. (2022), considers the production of γ -rays via the hadronic pion production by an outgoing wind that impacts the obscuring torus. As a third possibility, γ -rays could be produced in the radio jet by relativistic electrons that inverse-Compton scatter the infrared radiation from the torus (Lenain et al. 2010). The contribution of the jet to the γ -ray signal is also addressed in Tagawa et al. (2023).

In this work, we test the hypothesis that the jet of NGC 1068 contributes to the GeV γ -ray emission, based on radio observations of the jet and a physical model of the multi-wavelength non-thermal emission.

Radio observations (Gallimore et al. 2004; Michiyama et al. 2022) show distinct emission sites at some tens of parsecs, as well as a few hundreds of parsecs from the supermassive black hole of NGC 1068. These are commonly associated with its jet that is inclined to the line of sight (LoS) by about 45°. Hereof, the most distant emission site shows spatial widening, including four bright knot structures according to Michiyama et al. (2022), and the typical lobe structure that marks the head of the jet. Here the whole structure seems to have hit the interstellar medium (ISM) and, therefore, it presents an overall shock feature. Moreover, all of the observed radio structures can be inferred by spherical symmetric knot structures with a radius, r_k , on the order of about a few parsecs. According to Roy et al. (2000) these knots are streaming non-relativistically away from the central engine, with a speed of at most $v \sim 0.075c$.

Without accounting for the spatial features of the radio emission sites, Lenain et al. (2010) provided a phenomenological explanation of the observed γ -ray emission at GeV energies. They adopted an emission site at a distance from the torus of 65 pc, with a radius of $r_k = 7$ pc and a magnetic field of 0.1 mG, which, however, is not observed in the radio band. Using relativistic electrons with a broken power-law energy distribution they manage to explain observed GeV γ -rays by inverse

Compton (IC) scattering of IR photons from the torus. Based on the given radio power, the expected jet power P_{jet} according to Cavagnolo et al. (2010) is at the order of at most $10^{43} \text{ erg s}^{-1}$. Thus, the jet of NGC 1068 is comparably weak to produce the observed γ -ray luminosity between about 0.1 and 100 GeV of about $10^{41} \text{ erg s}^{-1}$.

In this work, we strive to account for the observational details of the individual radio knots and investigate if leptonic or hadronic emission in these knots can actually explain the observed γ -ray signal. The paper is structured as follows. In Sect. 2, we introduce the dominant emission scenarios for the previously introduced emission sites. In Sect. 3 we apply them to the case of NGC 1068. In Sect. 4, we conclude and discuss whether or not the observed radio knots can also be considered as origin of the observed γ -ray signal.

2. Theoretical toolbox

In the following, we introduce the potential leptonic and hadronic γ -ray production scenarios at the different location of the radio knots within the jet of NGC 1068, which have been observed by VLBA and ALMA. A schematic sketch of the different emission sites is shown in Fig. 1. As known from the jets of other AGN it is well established that these environments are suitable to accelerate electrons and protons to relativistic energies by, for instance, diffusive shock acceleration, shear acceleration, and/or magnetic reconnection (Matthews et al. 2020). However, we stay agnostic with respect to the acceleration mechanisms at work and presume a power-law distribution with a spectral index $q_{e,p}$ of relativistic electrons and protons, respectively, as a result of the acceleration.

2.1. Leptonic model

In the presence of a single relativistic electron (with $\beta \simeq 1$), its emitted synchrotron power is given by $P_{\text{syn}} = 4\sigma_T c \gamma_e^2 U_B / 3$, where σ_T denotes the Thomson cross section and $U_B = B^2 / 8\pi$ yields the magnetic energy density. Moreover, the spectral energy distribution (SED) of the emitted power shows a maximum at a frequency $\nu_{\text{syn}} \simeq \gamma_e^2 \nu_L$, with the characteristic Larmor frequency $\nu_L = eB / 2\pi m_e c$. In a similar manner, the total emitted power by IC scattering of a monochromatic photon target distribution with an energy density, U_{ph} , can also be given in the Thomson limit by $P_{\text{IC}} = 4\sigma_T c \gamma_e^2 U_{\text{ph}} / 3$. In addition, it is well known in the Thomson regime that an initial photon of a frequency, ν_0 , gives a mean frequency of $\nu_{\text{IC}} = 4\gamma_e^2 \nu_0 / 3$.

In the case of a differential energy distribution of electrons according to $n_e(\gamma_e) \propto \gamma_e^{-q_e}$, the emissivity $\epsilon(\nu)$ at a given frequency ν , within an interval $d\nu$, results for both emission processes from those electrons with an appropriate energy γ_e , within the interval $d\gamma_e$, so that

$$\epsilon_{\text{syn}}(\nu_{\text{syn}}) d\nu_{\text{syn}} \simeq \frac{1}{4\pi} P_{\text{syn}} \left(\gamma_e = \sqrt{\frac{\nu_{\text{syn}}}{\nu_L}} \right) n_e \left(\gamma_e = \sqrt{\frac{\nu_{\text{syn}}}{\nu_L}} \right) d\gamma_e, \quad (1)$$

and

$$\epsilon_{\text{IC}}(\nu_{\text{IC}}) d\nu_{\text{IC}} \simeq \frac{1}{4\pi} P_{\text{IC}} \left(\gamma_e = \sqrt{\frac{3\nu_{\text{IC}}}{4\nu_0}} \right) n_e \left(\gamma_e = \sqrt{\frac{3\nu_{\text{IC}}}{4\nu_0}} \right) d\gamma_e. \quad (2)$$

Hereby, we suppose that all the power is emitted at the frequencies ν_{syn} and ν_{IC} , respectively. This is an appropriate estimate

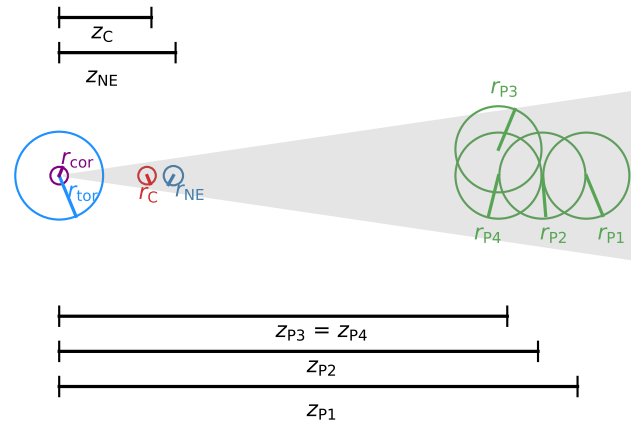


Fig. 1. Sketch of the environment, with the distances not shown to scale. The corona (in purple) has a radius of $r_{\text{cor}} \sim 10^{-4} \text{ pc}$. The torus (in light blue) has a radius of $r_{\text{tor}} = 3.6 \text{ pc}$. The C, NE, and P1–P4 knots are shown in red, dark blue, and green, respectively. The radii of the knots and respective distances, z , from the core are summarised in Table 1.

since the synchrotron and IC power spectra, for a given γ_e , show a peak at these characteristic frequencies. We note that these relations imply that all power is emitted at a typical frequency. With

$$\frac{d\gamma_e}{d\nu_{\text{syn}}} = \frac{\nu_{\text{syn}}^{-1/2}}{2\nu_L^{1/2}} \quad \text{and} \quad \frac{d\gamma_e}{d\nu_{\text{IC}}} = \frac{\nu_{\text{IC}}^{-1/2}}{2} \left(\frac{3}{4\nu_0} \right)^{1/2}, \quad (3)$$

the ratio of IC over synchrotron luminosity yields

$$\frac{\nu_{\text{IC}} L_{\nu_{\text{IC}}}}{\nu_{\text{syn}} L_{\nu_{\text{syn}}}} \equiv \frac{\nu_{\text{IC}} \epsilon_{\text{IC}}(\nu_{\text{IC}})}{\nu_{\text{syn}} \epsilon_{\text{syn}}(\nu_{\text{syn}})} = \left[\frac{3}{4} \frac{\nu_{\text{IC}} / \nu_0}{\nu_{\text{syn}} / \nu_L} \right]^{\frac{3-q_e}{2}} \frac{U_{\text{ph}}}{U_B}, \quad (4)$$

where the equality only holds in the Thomson limit, where $\nu_0 \nu_{\text{IC}} \ll (m_e c^2)^2 / h^2$. Hence, for a given target photon field (that is idealized to be monochromatic) and a known synchrotron flux spectrum at ν_{syn} , the resulting γ -ray luminosity $\nu_{\text{IC}} L_{\nu_{\text{IC}}}$ from IC scattering depends on the magnetic field strength according to $\nu_{\text{IC}} L_{\nu_{\text{IC}}} \propto B^{-(1+q_e)/2}$. We note that the exact calculation, without the delta approximation, leads to a slightly smaller ratio by about a factor of two in the range of interest. Thus, the previously introduced monochromatic luminosity ratio Eq. (4) provides, in any case, a robust upper limit of the actual ratio.

Supposing that the energy within the emission site is at equipartition, an estimate of the corresponding magnetic field strength can be derived in a way that is similar to the procedure published in Pacholczyk (1970). First, the total electron energy budget of those electrons that predominantly contribute to the synchrotron luminosity, $L_{\nu_{\text{syn}}}$, namely, those with $\gamma_e = \sqrt{\nu_{\text{syn}} / \nu_L}$ can be estimated by:

$$E_e \simeq m_e c^2 \frac{\nu_{\text{syn}}}{\nu_L} n_e \left(\gamma_e = \sqrt{\frac{\nu_{\text{syn}}}{\nu_L}} \right) V, \quad (5)$$

where V denotes the volume of the emission site. According to Eq. (1) the corresponding synchrotron luminosity can be approximated by:

$$\nu_{\text{syn}} L_{\nu_{\text{syn}}} \simeq \frac{1}{2} \left(\frac{\nu_{\text{syn}}}{\nu_L} \right)^{1/2} P_{\text{syn}} \left(\gamma_e = \sqrt{\frac{\nu_{\text{syn}}}{\nu_L}} \right) n_e \left(\gamma_e = \sqrt{\frac{\nu_{\text{syn}}}{\nu_L}} \right) V, \quad (6)$$

so that the total electron energy dependent on the differential synchrotron luminosity at ν_{syn} yields

$$E_e \simeq c_{\text{syn}} B^{-3/2} \nu_{\text{syn}} L_{\nu_{\text{syn}}} \quad \text{with} \quad c_{\text{syn}} = \frac{12\pi m_e c}{\sigma_T} \left(\frac{e}{2\pi m_e c \nu_{\text{syn}}} \right)^{1/2}. \quad (7)$$

With a magnetic field energy of $E_B = V U_B$, the total energy within the emission site is given by

$$E_{\text{tot}} = E_e + E_p + E_B = (1+k)c_{\text{syn}} B^{-3/2} \nu_{\text{syn}} L_{\nu_{\text{syn}}} + \frac{B^2 r_k^3}{6}, \quad (8)$$

where the heavy particle energy, E_p , is k times the electron energy of those electrons that predominantly contribute to $L_{\nu_{\text{syn}}}$. Its value depends on the acceleration mechanism of relativistic particles, but, in general, it is expected that $k \gg 1$. Assuming that the total energy is at its minimum, namely, $\partial E_{\text{tot}}/\partial B = 0$, we obtain a magnetic field strength of:

$$B_{\text{eq}} = (4.5)^{2/7} (1+k)^{2/7} c_{\text{syn}}^{2/7} r_k^{-6/7} \left(\nu_{\text{syn}} L_{\nu_{\text{syn}}} \right)^{2/7}, \quad (9)$$

for which the magnetic field energy is about equal to the total particle energy.

2.2. Hadronic model

In the case of a hadronic origin of the observed γ -ray luminosity, there is no robust low-energy counterpart (as in the leptonic scenario) that can be used to constrain the energy distribution of the CR protons. Moreover, γ -rays can in principle be produced by photomeson or hadronic pion production, namely, by inelastic interactions with some target gas and target photon field, respectively.

In the case of photomeson production, the corresponding photon emissivity is given by (Dermer & Menon 2009):

$$\tilde{\epsilon}_{\text{py}}(E_\gamma) = \frac{c \zeta_\gamma \sigma_{\text{py}}^{\text{s,m}}}{64\pi^2 \chi_\gamma m_p c^2} \frac{n_p(\bar{\gamma}_p)}{\bar{\gamma}_p^2} \int_{\epsilon'_l}^{\infty} d\epsilon \frac{n_{\text{ph}}(\epsilon)}{\epsilon^2} f(\bar{\gamma}_p, \epsilon), \quad (10)$$

where $n_{\text{ph}}(\epsilon)$ denotes the differential photon number density at a dimensionless photon energy $\epsilon = h\nu/m_e c^2$. Moreover, the function $f(\bar{\gamma}_p, \epsilon) \equiv \{[\min(2\bar{\gamma}_p \epsilon, \epsilon'_u)]^2 - \epsilon'_l{}^2\}$ accounts for single pion production, where $\sigma_{\text{py}}^{\text{s}} = 340 \mu\text{b}$, $\epsilon'_l = 390$, $\epsilon'_u = 980$, as well as multi-pion production, where $\sigma_{\text{py}}^{\text{m}} = 120 \mu\text{b}$, $\epsilon'_l = 980$, $\epsilon'_u \rightarrow \infty$. Furthermore, $\zeta_\gamma = 1$ and $\zeta_\gamma^{\text{m}} = 2$, respectively, denote the multiplicity in case of single and multi pion production respectively, and $\chi_\gamma^{\text{m,s}} = 0.1$ is the mean fractional energy of the produced γ -ray compared to the incident primary proton. In addition, $n_p(\bar{\gamma}_p)$ is the differential intensity of CR protons with a Lorentz factor $\bar{\gamma}_p \equiv (E_\gamma)/(\chi_\gamma m_p c^2)$.

In the case of hadronic pion production, the corresponding photon emissivity is given by (Schlickeiser 2002):

$$\tilde{\epsilon}_{\text{pp}}(E_\gamma) = \frac{2c n_{\text{gas}}}{3\pi m_\pi c^2} \int_{E_\gamma + \frac{m_\pi^2 c^4}{4E_\gamma}}^{m_\pi c^2 \gamma_{\text{p,max}}^{3/4}} dE_\pi \zeta \sigma_{\text{pp}} \left(\left(\frac{E_\pi}{m_\pi c^2} \right)^{4/3} \right) \times \left(\frac{E_\pi}{m_\pi c^2} \right)^{1/3} n_p \left(\left(\frac{E_\pi}{m_\pi c^2} \right)^{4/3} \right) [E_\pi^2 - m_\pi^2 c^4]^{-1/2}, \quad (11)$$

where n_{gas} denotes the constant target gas density. Moreover, the product of the total cross-section, σ_{pp} , and the multiplicity, ζ , can be approximated at $\gamma_p \geq 1.75$ by $\zeta \sigma_{\text{pp}}(\gamma_p) = 8.12 \times 10^{-27} (\gamma_p -$

$1)^{0.53} \text{ cm}^2$. We note that at $\gamma_p < 1.75$, the steep decline of the inclusive cross-section $\zeta \sigma_{\text{pp}}$ yields a strong suppression of the emissivity at sub-GeV energies.

Using a differential proton number density $n_p(\gamma_p) = n_0 (\gamma_p/\gamma_{0,p})^{-q_p}$ for $\gamma_{p,\text{min}} < \gamma_p < \gamma_{p,\text{max}}$, the associated total relativistic proton luminosity, $L_p \equiv 4\pi r_k^2 v_k m_p c^2 \int d\gamma_p \gamma_p n_p(\gamma_p)$, cannot exceed the available jet power P_{jet} , namely, $L_p = f_{\text{jet}} P_{\text{jet}}$ with $f_{\text{jet}} < 1$.

In this work, a homogeneous spherically symmetric emission site with a radius r_k is adopted, so that the γ -ray luminosity at a certain energy E_γ yields:

$$\nu_{\text{py}} L_{\nu_{\text{py}}} = A_{\text{py}} E_\gamma^2 \frac{c}{v_k} r_k f_{\text{jet}} P_{\text{jet}} \bar{\gamma}_p^{-q_p-2} \int_{\frac{\epsilon'_l}{2\bar{\gamma}_p}}^{\infty} d\epsilon \frac{n_{\text{ph}}(\epsilon)}{\epsilon^2} f(\bar{\gamma}_p, \epsilon), \quad (12)$$

and

$$\nu_{\text{pp}} L_{\nu_{\text{pp}}} = A_{\text{pp}} E_\gamma^2 \frac{c}{v_k} \left(\frac{n_{\text{gas}} r_k}{\text{cm}^{-2}} \right) f_{\text{jet}} P_{\text{jet}} \int_{E_\gamma + \frac{m_\pi^2 c^4}{4E_\gamma}}^{m_\pi c^2 \gamma_{\text{p,max}}^{3/4}} dE_\pi \times \left(\frac{E_\pi}{m_\pi c^2} \right)^{-\frac{4q_p-1}{3}} \left[\left(\frac{E_\pi}{m_\pi c^2} \right)^{\frac{4}{3}} - 1 \right]^{0.53} [E_\pi^2 - m_\pi^2 c^4]^{-\frac{1}{2}}, \quad (13)$$

respectively, with:

$$A_{\text{py}} = \frac{\zeta_\gamma \sigma_{\text{py}}^{\text{s,m}} (2 - q_p)}{48\pi m_p^2 c^4 \chi_\gamma (\gamma_{\text{p,max}}^{2-q_p} - \gamma_{\text{p,min}}^{2-q_p})}, \quad (14)$$

and

$$A_{\text{pp}} = \frac{2.89 \times 10^{-26} (2 - q_p)}{m_\pi m_p c^4 (\gamma_{\text{p,max}}^{2-q_p} - \gamma_{\text{p,min}}^{2-q_p})}. \quad (15)$$

The exponent of 0.53 in Eq. (13) results from the used energy dependence of the inclusive cross section. Dependent on the present target densities n_{gas} and n_{ph} , respectively, the hadronic γ -ray production is typically dominated by one of these processes. In the following, we introduce the photon target fields needed for the IC and photomeson scenarios.

2.3. Photon target

The broadband SED of NGC 1068 consists of different components. Some of its radio emission can be associated with synchrotron emission from the jet (Gallimore et al. 2004). The IR excess is predominantly due to thermal reradiation by dust particles in the vicinity of the torus (Raban et al. 2009; Lopez-Rodriguez et al. 2018). In the optical to UV band, we observe a ‘‘blue bump’’, which is interpreted as a pseudoblackbody emission from an optically thick and geometrically thin accretion disk. A soft X-ray excess and an underlying power-law mainly towards hard X-ray energies can be attributed to Comptonization of softer seed photons (Murase et al. 2020), which is typically associated with the AGN corona.

We show in Fig. 2 the target photon densities that are taken into account. In blue, we describe the dusty torus, with an average temperature of $T_{\text{tor}} \sim 150 \text{ K}$ (Lopez-Rodriguez et al. 2018). We used a simplified model with a blackbody spectrum as given by:

$$\nu L_\nu^{\text{tor}} = \frac{L_{\text{bol}}}{6} \left(\frac{h\nu(1+z)}{k_B T_{\text{tor}}} \right)^4 \exp\left(-\frac{h\nu(1+z)}{k_B T_{\text{tor}}}\right), \quad (16)$$

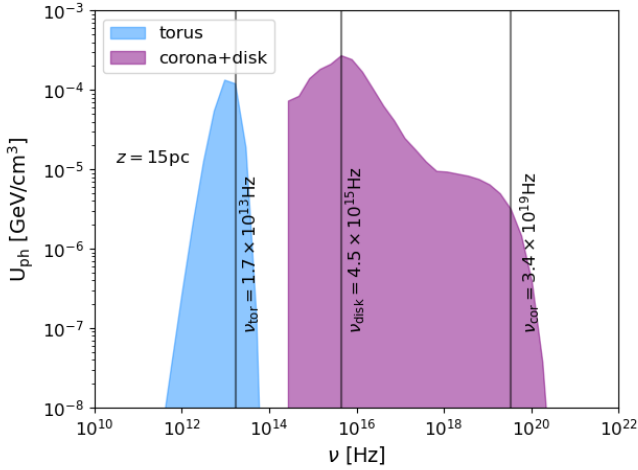


Fig. 2. SED of the energy density within the torus and corona+disk environment, computed at a distance of 15 pc. The torus field has its peak at a characteristic frequency of $\nu_{\text{tor}} = 1.7 \times 10^{13}$ Hz, the disk at a frequency of $\nu_{\text{disk}} = 4.5 \times 10^{15}$ Hz and the corona at a frequency of $\nu_{\text{cor}} = 3.4 \times 10^{19}$ Hz.

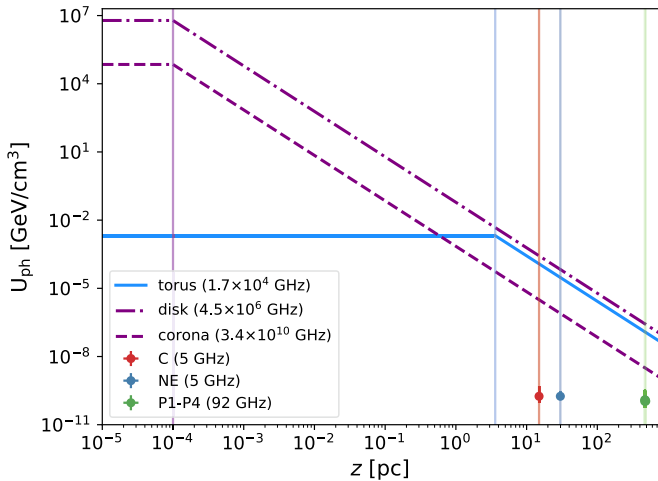


Fig. 3. Differential photon energy densities at their characteristic frequencies. The data points for knot C and NE refer to the internal background photon energy densities according to Gallimore et al. (2004) (at 5 GHz) and the ones for P1-P4 refer to the data from Michiyama et al. (2022) (at 92 GHz). For the conversion of the radio data of the six knots knot radii of $r_{k,1} = 0.2 \pm 0.1$ pc, $r_{k,2} = 0.3 \pm 0.15$ pc and $r_{k,3} = 3.5 \pm 1.75$ pc, respectively, are assumed.

which properly explains the spectral emission around the peak at about $\nu_{\text{tor}} = 1.7 \times 10^{13}$ Hz; however, at $\nu \gg \nu_{\text{tor}}$, the additional contribution by the clumpy torus and star formation become dominant (see, e.g., Lopez-Rodriguez et al. 2018). Here the prefactor of 1/6 ensures that the integral over L_{ν}^{tor} yields the bolometric luminosity of $L_{\text{bol}} = 2.46 \times 10^{44}$ erg s $^{-1}$, as provided by the so-called CLUMPY torus model by Lopez-Rodriguez et al. (2018), where an outer radius of $r_{\text{tor}} = 3.6$ pc has been adopted¹. We note that the alternative scenario of a smooth torus yields a photon density that is about a factor of 0.5 times smaller.

In purple, we illustrate the photon energy density originating from the innermost central region, that consists of the disk and the corona, which can extend up to ~ 100 Schwarzschild

radii (Murase 2022), which is $\sim 10^{-4}$ pc in the case of NGC 1068. Hereby we model the photon field of the accretion disk by using an empirical model by Ho (2008), where the UV spectrum is determined from the given Eddington ratio $\lambda_{\text{Edd}} \equiv L_{\text{bol}}/L_{\text{Edd}} \sim 1.4$ of NGC 1068. Since different spatial scales are to be taken into account, we cut off the spectrum at energies lower than 2.4×10^{14} Hz. The main contribution of infrared photons at these energies originate predominantly from outside the corona+disk environment such as from the outer star formation region and the torus (see also Elvis et al. 1994; Murase et al. 2014).

The subsequent coronal X-ray spectrum is modelled by a power-law with an exponential cutoff. Here, the photon index, Γ_X , is correlated to λ_{Edd} through $\Gamma_X \approx 0.167 \times \log(L_{\text{Edd}}) + 2$ and the cutoff energy is given by $E_{X,\text{cut}} \sim [-74 \log(\lambda_{\text{Edd}}) + 1.5 \times 10^2]$ keV (Murase et al. 2020).

We note that this emission from the nuclear region of NGC 1068 gets reprocessed and/or scattered by the clouds in the broad line region, so that a fraction $f_{\text{diff}} \ll 1$ of the central luminosity $\nu_0 L_{\nu_0}$ forms a diffuse radiation field at a distance from the BH of $z \sim 0.1$ pc. However, at the considered emission sites, where $z \gg 1$ pc, this diffuse photon field appears again as a point source yielding a photon energy density in the reference frame of the knot of (Dermer & Menon 2009):

$$U_{\text{trg}} = \frac{\nu_0 L_{\nu_0}}{4\pi z^2 c} \left[\Gamma_k^2 (1 + \beta_k)^2 \right]^{-1}, \quad (17)$$

where $\beta_k c$ denotes the velocity of the knot and Γ_k is its corresponding Lorentz factor. We note that at small distances from the isotropic photon target, the previous point source assumption is no longer valid and details of the geometry of the isotropic radiation field have to be taken into account to obtain the photon energy density in the reference frame of the knot. We refer to Sikora et al. (1994) for more details. Since all of the considered emission sites show non-relativistic velocities with $\beta_k \equiv v_k/c \lesssim 0.05$ (Roy et al. 2000), we can neglect these relativistic beaming effects in the following. We note that Eq. (17) can also be used for the isotropic photon field from the torus, with a luminosity, $\nu_0 L_{\nu_0}$, if we assume that $z \gg r_{\text{tor}}$ and the spatial extension of the torus is not orders of magnitudes smaller than r_{tor} . As shown in Fig. 3 the photon energy density from the corona+disk environment is at all distances larger than the differential photon density of the torus at its peak frequency of $\nu_{\text{tor}} = 1.7 \times 10^{13}$ Hz. Moreover, it is shown in Fig. 3 for the considered emission sites with a knot radius r_k as well as an observed luminosity $\nu_{\text{obs}} L_{\text{obs}}$ in the radio band, as given in Table 1, that the internal photon field² energy density at ν_{obs} yields:

$$U_{\text{trg}}^{(\text{int})} = \frac{\nu_{\text{obs}} L_{\text{obs}}}{4\pi r_k^2 c} \ll U_{\text{trg}}. \quad (18)$$

This also holds for the considered emission sites if we account for the observed spectral behaviour, α , and compare the energy densities at the characteristic frequencies of the torus or the disk. Hence, in the following, only the external photon fields are taken into account, as the dominant photon target to generate γ -rays up to some tens of GeV.

In general, the γ -ray luminosity, according to Eqs. (4), (12), and (13), scales linearly with the present target photon density, if absorption via $\gamma\gamma$ pair production (with an absorption coefficient $\alpha_{\gamma\gamma}$) can be neglected. Figure 4 shows that this is actually a

¹ Under consideration of the different assumptions on the distance of NGC 1068.

² With internal we are referring to the photon density that is produced within the considered knot structures, in contrast to the previously discussed external fields.

Table 1. Properties for the different emission sites that have been observed in the radio band by Gallimore et al. (2004) (for C and NE) and Michiyama et al. (2022) (for P1–4) as well as the expected magnetic field strength according to Eq. (9).

	z [pc]	r_k [pc]	ν_{obs} [GHz]	$\nu_{\text{obs}}L_{\nu_{\text{obs}}}$ [$10^{36} \text{ erg s}^{-1}$]	α	$B_{\text{eq}}(k = 100)$ [mG]
C	15	0.2	5	6.4	0.23	15.4
NE	30	0.3	5	9.5	0.90	10.9
P1	484	3.5	92	7.6	0.50	1.40
P2	477	3.5	92	8.6	0.59	1.40
P3	468	3.5	92	8.8	0.65	1.40
P4	468	3.5	92	7.5	0.50	1.40

Notes. Length scales are determined supposing a source distance of 10.1 Mpc, so that $1'' = 49 \text{ pc}$. Here, z is the distance of the knot with respect to the central engine, r_k is the knot radius, $\nu_{\text{obs}}L_{\nu_{\text{obs}}}$ is the observed radio luminosity at a frequency, ν_{obs} , and α the spectral index at this frequency.

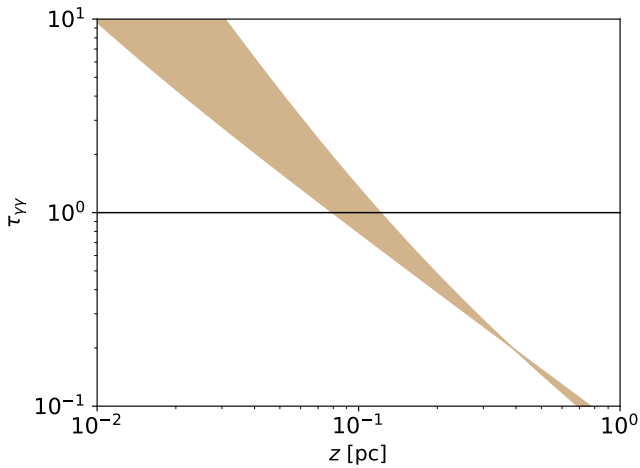


Fig. 4. Optical thickness, $\tau_{\gamma\gamma}$, at 17 GeV dependent on the distance z of the knot with respect to the central engine. Here, the absorption coefficient, $\alpha_{\gamma\gamma}$, is calculated according to Dermer & Menon (2009) and the shaded range corresponds to the uncertainty of the knot radius evolution (see e.g., Zacharias et al. 2022 for more details).

proper presumption as even at the highest considered γ -ray energies the corresponding optical thickness $\tau_{\gamma\gamma} \equiv \alpha_{\gamma\gamma} r_k \ll 1$ for the considered radio knots. Moreover, it illustrates that dependent on the supposed knot radius evolution the observed γ -rays at a few $\times 10$ GeV cannot be explained by alternative emission sites that are closer than about a few $\times 0.1$ pc to the central nucleus.

3. Results

3.1. Leptonic scenario

In the following, we determine the γ -ray luminosity at the low and high-energy end of the recently updated *Fermi*-LAT flux (Abdollahi et al. 2022), namely, at $\nu_{\text{IC},1} = 0.18 \text{ GeV } h^{-1}$ (luminosity of $1.7 \times 10^{40} \text{ erg/s}$) and $\nu_{\text{IC},2} = 17 \text{ GeV } h^{-1}$ (luminosity of $8.2 \times 10^{39} \text{ erg s}^{-1}$). Hereby, we use Eq. (4) to determine the γ -ray luminosity from IC scattering in the Thomson limit, so that

$$\nu_{\text{IC}}L_{\nu_{\text{IC}}} = 2 \left[\frac{3}{8\pi} \frac{\nu_{\text{IC}}/\nu_0}{\nu_{\text{syn}}} \frac{e}{m_e c} \right]^{\frac{3-q_e}{2}} \frac{\nu_0 L_{\nu_0}}{z^2 c} B^{-\frac{1+q_e}{2}} \nu_{\text{syn}} L_{\nu_{\text{syn}}}, \quad (19)$$

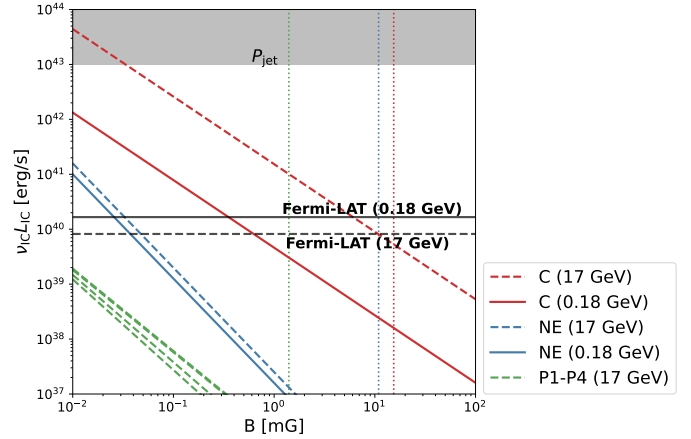


Fig. 5. Produced luminosity via IC process, according to Eq. (4). The dotted lines indicate the values of the magnetic field according to Eq. (9). The grey shaded band excludes all values higher than P_{jet} .

where $\nu_{\text{syn}}L_{\nu_{\text{syn}}} = \nu_{\text{obs}}L_{\nu_{\text{obs}}}$ at $\nu_{\text{syn}} = \nu_{\text{obs}}$ as given in Table 1. A maximal γ -ray luminosity is obtained for a dense target energy distribution at ν_0 as well as a low value of ν_0 in case of $q_e < 3$. In case of optically thin synchrotron emission at ν_{syn} according to $L_{\nu_{\text{syn}}} \propto \nu_{\text{syn}}^{-\alpha}$ the spectral behavior of the relativistic electron distribution can be determined by $q_e = 2\alpha + 1$. We note that this spectral behavior can in principle become softer towards higher energies due to the impact of synchrotron or IC losses. Without these softening effects, the spectral behavior as given in Table 1 indicates that the torus with a spectral luminosity of $\nu_0 L_{\nu_0} = 1.72 \times 10^{44} \text{ erg s}^{-1}$ at $\nu_0 = \nu_{\text{tor}} = 1.7 \times 10^{13} \text{ Hz}$ is the dominant photon target.

As shown in Fig. 5 the emission sites C is at $\nu_{\text{IC},2} = 17 \text{ GeV } h^{-1}$ able to exceed the observed γ -ray luminosity for the whole range of reasonable magnetic field strength values, such as its B_{eq} value (for a proton-to-electron energy ratio of $k = 100$) that is indicated by the red dotted line. We note that for all emission sites the values of B_{eq} are rather large. Comparing the results at 0.18 and 17 GeV, it is clear that the adopted spectral behavior of the relativistic electrons, which has been derived from the radio emission, is too hard with respect to the observed spectral behavior in the γ -ray band. Thus, in principle this emission site has enough total energy to produce the observed γ -rays above about a few GeV, if electrons can be accelerated up to $\gamma_e \approx \sqrt{3\nu_{\gamma}/4\nu_{\text{tor}}} \approx 4 \times 10^5$. To explain also the sub-GeV γ -ray emission, a magnetic field strength of about 0.5 mG is needed, which is about an order of magnitude smaller than what is expected from the minimal total energy estimate. Moreover, a significant softening of the spectral behavior of the CR electrons to an index of $q_e \sim 3.3$ at $\gamma_e \approx \sqrt{3\nu_{\text{IC},1}/4\nu_{\text{tor}}} = 4 \times 10^4$ is needed to agree with the spectral behavior of the observed γ -ray data.

Hence, in addition to the low magnetic field strength, the data also shows the need for a strong cooling break in the electron spectrum at about 1 GeV. As shown in Fig. 6, a break at about these energies can only occur if the escape of CR electrons is delayed by at least an order of magnitude with respect to the free streaming condition which is determined by the light-crossing time of the knot, suggested to be about 0.2 pc by VLBA observations (cf. Table 1). This can in principle be realized by diffusive escape from the knot, which however, already softens the initial spectral behavior so that only a minor softening by $\Delta q_e \approx 0.6$ emerges at the transition from diffusive escape to IC losses. Moreover, we can see that synchrotron emission

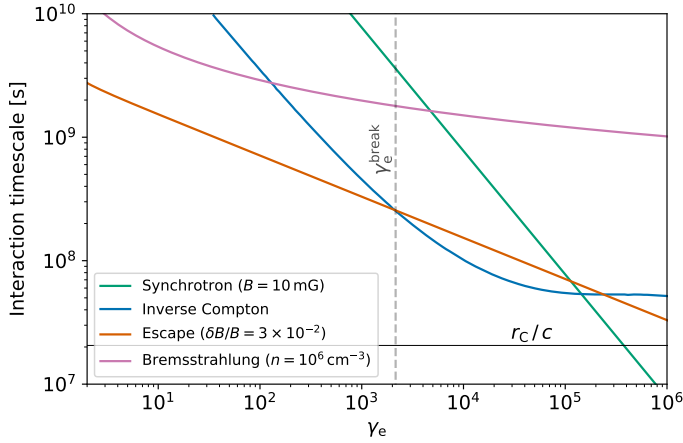


Fig. 6. Interaction timescales for the relevant radiative processes in C knot. The horizontal black line represents the size of the region based on radio observations. We can see that inverse Compton cooling (blue curve) becomes efficient for electron energies $E_e > 1.1$ GeV, as denoted by the vertical line, leading to a cooling break in the electron spectrum.

(green line) is comparatively inefficient, since the energy density of the magnetic field is much lower than that of the external thermal fields. That also applies to relativistic bremsstrahlung losses (purple line), even for the case of a dense target plasma. Moreover, as shown previously in Fig. 4, at distances of ~ 10 pc there is a low opacity to gamma-gamma annihilation, therefore the source is considered to be optically thin. Thus, all potential interaction processes in knot C are not able to explain the necessary softening of the spectrum. A significant γ -ray contribution from the NE knot is only obtained for a magnetic field strength $\ll 0.1$ mG. Furthermore, it can be excluded that the observed γ -rays originate from the head of the jet (i.e., P1–4).

3.2. Hadronic scenario

Accounting for the external photon targets by the torus, disk and corona with a differential photon number density,

$$n_{\text{ph}}(\epsilon) = \frac{1}{4\pi} \frac{m_e c^2}{(h\nu_0)^2} U_{\text{trg}}, \quad (20)$$

at a dimensionless photon energy $\epsilon = h\nu_0/m_e c^2$, we determine in the following the resulting γ -rays according to photomeson production as given by Eq. (12). Since the torus only provides photons at energies $\ll 100$ keV, these target photons are not energetic enough to provide γ -rays up to some tens of GeV. However, the X-ray photons from the corona with energies up to few $\times 100$ keV are in principle energetic enough to yield γ -rays at these energies, but not at sub-GeV energies. Moreover, $v_{\pi\gamma} L_{\nu_{\pi\gamma}}$ is (even for the most optimistic scenarios) also at 17 GeV multiple order of magnitudes below the observations as illustrated by the pale color bands in Fig. 7. Hence, we can clearly rule out that the jet produces the observed γ -rays by a photohadronic scenario.

In the case of hadronic pion production the dark color bands in Fig. 7 show that at a few GeV, the resulting luminosity $v_{\text{pp}} L_{\text{pp}}$ is much closer to observations than the photohadronic scenario. At the same time, due to the steep decline of the inclusive cross section for π^0 production at $\gamma_p \leq 1.75$, the resulting γ -ray flux will also decline below ~ 1 GeV; so that, in any case, the observed sub-GeV γ -rays cannot be explained. In order to match the observed γ -ray luminosity at 17 GeV, the Fig. 8 shows the necessary product of target gas density (n_{gas}) and the

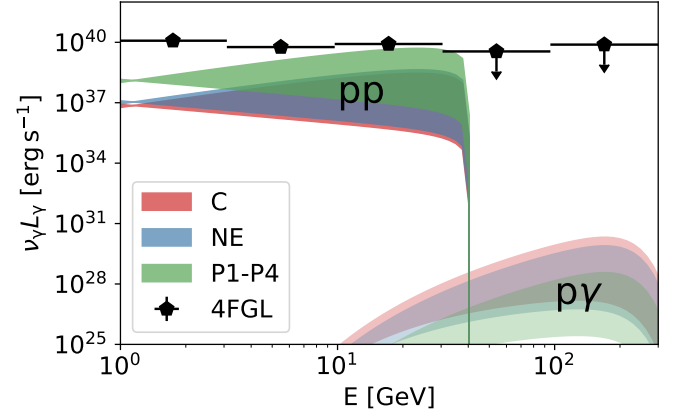


Fig. 7. Range of the hadronic γ -ray flux from photomeson production (pale color bands) and hadronic pion production (dark color bands) for spectral indices $q_p \in [1, 3]$. Here a knot velocity of $v_b = 0.075 c$, as well as a target gas density of $n_{\text{gas}} = 10^3 \text{ cm}^{-3}$ and $f_{\text{jet}} = 0.5$ is used. Moreover, we adopted $\gamma_{p,\text{min}} = 1$ and $\gamma_{p,\text{max}} = 2 \times 10^3$ to obtain a cut-off in the resulting γ -ray flux from hadronic pion production at about a few $\times 10$ GeV as indicated by the observations.

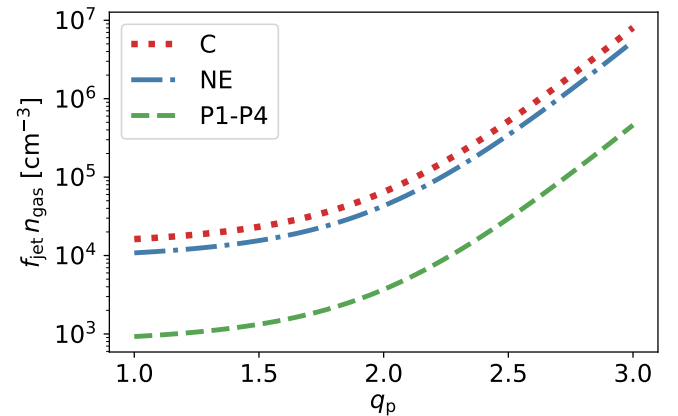


Fig. 8. Necessary parameter condition for the different knot environments C, NE, and P1–P4 to explain the observed γ -ray flux of $8.2 \times 10^{39} \text{ erg s}^{-1}$ at 17 GeV by hadronic pion production. Here a knot velocity of $v_b = 0.075 c$ is used as well as $\gamma_{p,\text{min}} = 1$ and $\gamma_{p,\text{max}} = 2 \times 10^3$ to obtain a cut-off in the resulting γ -ray flux at about a few $\times 10$ GeV as indicated by the observations.

fraction (f_{jet}) of the jet power that goes into CR protons dependent on their spectral index (q_p). Even in the most optimistic scenario where the jet is completely dominated by the CR protons, namely, $f_{\text{jet}} \approx 1$, the target gas density needs to be multiple orders of magnitude higher than the average ISM density of about 1 cm^{-3} . As shown by García-Burillo et al. (2014), dense molecular gas with $n(\text{H}_2) \geq 10^{5-6} \text{ cm}^{-3}$ is present within the circumnuclear disk of NGC 1068. In particular, knot C seems to impact a giant molecular cloud (Gallimore et al. 2004), which is (in part) due to the need of free-free absorption at 1.4 GHz. Thus, if the target gas in the considered knot structures also shows an increased density, the slight excess of the observed γ -ray flux at about 17 GeV could actually be a result of the contribution from γ -rays by hadronic pion production. In any case, an additional γ -ray emitter is also needed to explain the observed γ -rays at sub-GeV energies.

4. Discussion and conclusions

In this work, we discuss the possibility that the different radio emission sites, so-called knots, within the jet-like structure of NGC 1068 can be associated as the origin of the observed γ -ray flux between about 0.1 and 100 GeV. Hereby, we account for the observed spatial and spectral details of these radio structures and discuss the potential leptonic and hadronic γ -ray emission scenarios.

For relativistic protons within these radio knots, hadronic pion production is the most promising scenario to explain the mild excess of the observed γ -ray flux at about 17 GeV. For this purpose, it is needed that

$$\left(\frac{v_b/c}{0.075}\right)^{-1} \left(\frac{n_{\text{gas}}}{1 \text{ cm}^{-3}}\right) \left(\frac{r_k}{5 \text{ pc}}\right) \left(\frac{f_{\text{jet}} P_{\text{jet}}}{10^{43} \text{ erg s}^{-1}}\right) \sim 10^{2-3};$$

hence, the target gas needs to be significantly denser than in the average ISM. In particular the knot C shows indications of the impact of a dense molecular cloud (Gallimore et al. 2004) that would be sufficient to explain the GeV γ -rays. But in any case, an additional leptonic γ -ray contribution is needed to account for the observed sub-GeV γ -rays. This result is also in agreement with Fang et al. (2023), who provides a similar outcome for gas densities of $n_{\text{gas}} \sim 10^5 \text{ cm}^{-3}$ and hard proton spectra. Moreover, this could be a possible explanation of the few $\times 100$ GeV emission observed by Ajello et al. (2023).

For relativistic electrons, IC scattering with the IR photons from the torus yields the highest flux of γ -rays based on the expected spectral behavior of the electrons from radio observations. Depending on the supposed magnetic field strength within these radio knots, we could constrain that the knot C, which is the closest with respect to the central engine, represents the most likely emission site for the production of the observed γ -rays. However, for this purpose, it is necessary for: (i) the magnetic field strength to be $\lesssim 1$ mG; and (ii) the electron spectrum needs to show a break with a strong softening at about an energy of (1–10) GeV to agree with the observed spectral behavior of the γ -ray flux. However, we also show that such a strong softening (by $\Delta q_e \simeq 1.8$ if at low energies $q_e \simeq 1.5$ as indicated from VLBA observations) cannot emerge from the potential interaction processes in knot C. In general, these findings are in good agreement with the results from Lenain et al. (2010); however, the previously mentioned conditions (i) and (ii) were assumed to explain the γ -ray data by IC scattering with IR photons from the torus in that work. Still, these conditions do not hold, because the radius and magnetic field values needed to achieve the right γ -ray luminosity are ~ 0.1 pc and 0.1 mG. These values are, respectively, an order of magnitude lower and higher than what is observed and expected. Moreover, we do not naturally find a spectral break at an energy of (1–10) GeV. Therefore, by accounting for the observational constraints by Gallimore et al. (2004), it is not possible to explain the observed γ -rays by the radio knot C or any other observed knot structure. Yet, if one of these sites impacts a dense target gas, they could still provide some hadronic γ -ray contribution at about 10 GeV.

One of the key parameters of these results is the strength of the magnetic field: based the minimal total energy condition, as given in Eq. (9), a value of about $(1+k)^{2/7}$ mG is obtained; however, this still includes the uncertain proton-to-electron energy ratio, k . Moreover, this classical estimate can be revised, because it does not account for inhomogeneous magnetic fields, the synchrotron spectrum over the real energy range and the real ratio, k , of total energies. Using the number density ratio (instead of the hardly known energy ratio, k) for the same value of 100, it has been

shown by Beck & Krause (2005) that it is only for soft spectra (e.g., the case of knot NE with $\alpha \simeq 0.90$), the resulting magnetic field strength can become smaller by about a factor of about 0.4. Hence, even in the most extreme scenario of a vanishing hadronic particle energy (so that $k \simeq 0$), the field strengths, B_{eq} , given in Table 1, would only become smaller by a factor of about 0.27.

Further, knot C only manages to produce sufficient γ -rays due to its non-relativistic bulk motion. In the case of a mildly relativistic motion, namely, $\Gamma_b \gg 1$, the target photon energy density in the rest frame of the knot would be reduced according to Eq. (17) and the target photon frequency, ν_0 , would suffer from relativistic Doppler de-boosting; in total, this would lower the expected IC γ -ray luminosity by a factor of $\Gamma_b^{-(1+q_e)/2}$.

Apart from the previously discussed spatially resolved radio knots, there could be the chance that the observed γ -rays are produced much closer to the foot of jet, where radio telescopes cannot resolve individual emission sites. As shown in Fig. 4, the emission sites already become opaque for ~ 10 GeV γ -rays at distances of about 0.1 pc due to $\gamma\gamma$ pair production. Therefore, such alternative emission sites are not sufficient to explain the observed γ -rays at the highest energies.

Acknowledgements. We acknowledge funding from the German Science Foundation DFG, within the Collaborative Research Center SFB 1491 ‘‘Cosmic Interacting Matters – From Source to Signal’’. X.R. is supported by the DFG through grant SFB 1258 ‘‘Neutrinos and Dark Matter in Astro- and Particle Physics’’ and by the Excellence Cluster ORIGINS, which is funded by the DFG under Germany’s Excellence Strategy – EXC 2094 – 390783311.

References

- Abbasi, R., Ackermann, M., Adams, J., et al. 2022, *Science*, **378**, 538
 Abdollahi, S., Acero, F., Baldini, L., et al. 2022, *ApJS*, **260**, 53
 Ackermann, M., Ajello, M., Allafort, A., et al. 2012, *ApJ*, **755**, 164
 Ajello, M., Murase, K., & McDaniel, A. 2023, *ApJ*, **954**, L49
 Beck, R., & Krause, M. 2005, *Astron. Nachr.*, **326**, 414
 Cavagnolo, K., McNamara, B., Nulsen, P., et al. 2010, *ApJ*, **720**, 1066
 Dermer, C. D., & Menon, G. 2009, *High Energy Radiation from Black Holes: Gamma Rays, Cosmic Rays, and Neutrinos* (Princeton: Princeton University Press)
 Eichmann, B., Oikonomou, F., Salvatore, S., Dettmar, R.-J., & Tjuz, J. B. 2022, *ApJ*, **939**, 43
 Elvis, M., Wilkes, B. J., McDowell, J. C., et al. 1994, *ApJS*, **95**, 1
 Fang, K., Rodriguez, E. L., Halzen, F., & Gallagher, J. S. 2023, *ApJ*, **956**, 8
 Gallimore, J. F., Baum, S. A., & O’Dea, C. P. 2004, *ApJ*, **613**, 794
 García-Burillo, S., Combes, F., Usero, A., et al. 2014, *A&A*, **567**, A125
 Ho, L. C. 2008, *ARA&A*, **46**, 475
 Inoue, Y., Khangulyan, D., & Doi, A. 2020, *ApJ*, **891**, L33
 Inoue, S., Cerruti, M., Murase, K., & Liu, R.-Y. 2022, *Phys. Rev. Lett.*, submitted [arXiv:2207.02097]
 Kheirandish, A., Murase, K., & Kimura, S. S. 2021, *ApJ*, **922**, 45
 Lenain, J. P., Ricci, C., Türler, M., Dorner, D., & Walter, R. 2010, *A&A*, **524**, A72
 Lopez-Rodriguez, E., Fuller, L., Alonso-Herrero, A., et al. 2018, *ApJ*, **859**, 99
 Matthews, J. H., Bell, A. R., & Blundell, K. M. 2020, *Nat. Rev.*, **89**, 101543
 Michiyama, T., Inoue, Y., Doi, A., & Khangulyan, D. 2022, *ApJ*, **936**, L1
 Murase, K. 2022, *ApJ*, **941**, L17
 Murase, K., Inoue, Y., & Dermer, C. D. 2014, *Phys. Rev. D*, **90**, 023007
 Murase, K., Kimura, S. S., & Mészáros, P. 2020, *Phys. Rev. Lett.*, **125**, 011101
 Pacholczyk, A. 1970, *Radio Astrophysics* (San Francisco: W.H. Freeman & Co)
 Raban, D., Jaffe, W., Röttgering, H., Meisenheimer, K., & Tristram, K. R. 2009, *MNRAS*, **394**, 1325
 Roy, A. L., Wilson, A. S., Ulvestad, J. S., & Colbert, J. M. 2000, EVN Symposium 2000, Proceedings of the 5th european VLBI Network Symposium, eds J.E. Conway, A.G. Polatidis, R.S. Booth & Y.M. Pihlström (Onsala Space Observatory), 7
 Schlickeiser, R. 2002, *Cosmic Ray Astrophysics* (Berlin: Springer)
 Seyfert, C. K. 1943, *ApJ*, **97**, 28
 Sikora, M., Begelman, M. C., & Rees, M. J. 1994, *ApJ*, **421**, 153
 Tagawa, H., Kimura, S. S., & Haiman, Z. 2023, *ApJ*, **955**, 23
 Tully, R. B., Rizzi, L., Shaya, E. J., et al. 2009, *AJ*, **138**, 323
 Zacharias, M., Reimer, A., Boisson, C., & Zech, A. 2022, *MNRAS*, **512**, 3948